Journal of Alloys and Compounds 853 (2021) 156892

Contents lists available at ScienceDirect

Journal of Alloys and Compounds

journal homepage: http://www.elsevier.com/locate/jalcom

Enhancing surface properties of (Fe,Cr)Al − Al_2O_3 nanocomposite by oxygen ion implantation

F. Sourani [a, b, *], M.H. Enayati [a], F. Ashrafizadeh [a], F.S. Sayyedan [a], P.K. Chu [c]

[a] Department of Materials Engineering, Isfahan University of Technology, Isfahan 84156-83111, Iran
[b] Department of Mechanical Engineering, University of Hong Kong, Hong Kong, China
[c] Department of Physics, Department of Materials Science & Engineering, and Department of Biomedical Engineering, City University of Hong Kong, Tat Chee Avenue, Kowloon, Hong Kong, China

ARTICLE INFO

Article history:
Received 17 June 2020
Received in revised form
12 August 2020
Accepted 25 August 2020
Available online 28 August 2020

Keywords:
Oxygen ion implantation
(Fe,Cr)Al− Al_2O_3 nanocomposite
Nanoindentation behavior
Oxidation resistance

ABSTRACT

Ion implantation has been used as a surface treatment technique on (Fe,Cr)Al-10%vol Al_2O_3 nanocomposite to enhance its surface properties. The process was carried out at 150 kV with an oxygen dose of 1×10^{18} ions/cm^2 at room temperature. Microstructural characterization and phase composition were performed by scanning electron microscopy (SEM), transmission electron microscopy (TEM) and X-ray diffraction (XRD) of the Al_2O_3 layer formed on the nanocomposite surface. Mechanical properties measurements including hardness, fracture toughness and coefficient of friction were studied. Nanoindentation tests demonstrated an increase of 50% in the hardness value after ion implantation. Fracture toughness increased to a value of 21.3 ± 0.9 MPa m$^{1/2}$ after O_2 ion implantation. Scratch test results revealed an improvement in tribological behavior of the oxygen implanted surface compared to the unimplanted substrate. Cyclic oxidation tests, at 1100 °C, revealed that oxygen ion implantation slightly improved high temperature oxidation resistance of the nanocomposite.

1. Introduction

Nanocomposites based on iron aluminides with high strength, resistance to oxidation and sulfidation, high melting point and low density, have been considered as a new group of advanced engineering materials of rather low cost during the recent years. Several approaches have been introduced to improve properties of these aluminides including micro-alloying, surface modification and incorporation of second phase particles [1–3]. In order to improve high-temperature strength of intermetallic alloys, ceramic particles may be utilized to form reinforcement phases [4–7]; many researchers have confirmed the positive effect of chromium and Al_2O_3 particles on mechanical properties of Fe_3Al intermetallic compound. Aghili et al. [8] used cold isostatic pressing to produce bulk $(Fe,Cr)_3Al$ nanocomposite samples with an average microhardness of 626 HV, which was about twice greater than that for the Fe_3Al-20 vol% Al_2O_3 composite prepared by other methods [9]. Bai et al. [10] reported that corrosion resistance of Fe(Al)−Al_2O_3 was affected slightly by adding 20 wt% Al_2O_3. Further, it was found that corrosion resistance of composites was improved with addition of 4 wt% chromium.

Ion implantation is an effective technique for improving the surface properties of materials such as hardness, wear resistance and corrosion behavior [11]. Guseva et al. [12] used the implantation of oxygen ions to enhance the wear resistance of various WC-Co tools. The main advantages of ion implantation are the possibility of introducing any element into a solid target at low processing temperatures [13]. In plasma ion-implantation, specific ions (N_2, O_2, H_2, etc.) are implanted into the surface of a solid, resulting in a change of chemical composition on the surface to a depth of around 100 nm. Negatively biased samples are placed in a high-density plasma chamber, where ions in the plasma are accelerated towards the surface to be implanted. The process has been shown to provide strong adhesion of implanted layer to the substrate where extremely high solubility of ions can be achieved. Since process temperatures are often low, the dimensions of the components and bulk properties retained unaltered, while the treatment of complex shapes is also possible by manipulation of the substrate.

Ion implantation offers a versatile means of producing surface

* Corresponding author. Department of Materials Engineering, Isfahan University of Technology, Isfahan 84156-83111, Iran.
E-mail address: f.sourani@ma.iut.ac.ir (F. Sourani).

https://doi.org/10.1016/j.jallcom.2020.156892
0925-8388/

layers with controlled compositions in composite materials and metals, without altering grain structure of material [13–18]. Barison et al. [15] indicated that ion implantation of manganese in silica glass leads to the formation of a variety of compounds. In the sample irradiated with 1×10^{16} Mn^{+} ions cm^2, the in-depth deviation of the O/Si ratio from the stoichiometric value of silica was almost insignificant while Mn implanted atoms react with silica to form manganese silicate, $MnSiO_3$. Shanaghi et al. [19] enhanced the mechanical and corrosion resistance of TiAl by Cr-ion implantation. They produced a uniform, smooth, and crack-free surface layer with a thickness of 50 nm, also changes the roughness, hardness, and elastic modulus from 17.4 nm, 64.31 GPa, and 2.74 GPa for the pristine NiTi alloy to 6.1 nm, 89.27 GPa, and 4.77 GPa of the ion-implanted sample, respectively.

Loinaz et al. [20] studied the effects of N_2 ion-implantation on mechanical properties, wear resistance and structure of Ti6Al4V. They demonstrated that ion implantation effectively improved surface hardness and abrasive wear resistance of the material. Ion-implantation of light elements, such as nitrogen, carbon or oxygen into Ti6Al4V, lead to an increase in hardness due to the formation of hard precipitates. Various studies also emphasize the effect of the ion implantation on creating a hard phase with corrosion resistance [21–25]. Ryabchikov et al. [26] modified Al by high-intensity low-energy Ti-ion implantation. Results illustrated that the hardness of the surface layer increased from 0.4 GPa (undoped Al) to 3.5–4 GPa, while the wear resistance increased by more than an order of magnitude. Also, Marcondes et al. [27] used ion implantation on UHMWPE polymer and reported a wear rate of 1041×10^{-8} mm^3/Nm after ion-implantation which was significantly lower (200%) than that obtained for untreated material, with a wear rate of 3045×10^{-8} mm^3/Nm. Similarly, a threefold increase in wear resistance of UHMWPE has been reported when sliding against 316L stainless steel, the improvement was attributed to N_2 ion induced surface hardening as a result of cross-linking [28].

In our previous work, the successful synthesis of FeAl, (Fe,Cr)Al and (Fe,Cr)Al - 5 and 10% Al_2O_3 nanocomposites was reported [29]. In addition, it was inferred that optimum properties in terms of hardness, fracture toughness and creep resistance were obtained for (Fe,Cr)-10%vol Al_2O_3 nanocomposite. For effective use of these composite materials, in many applications, surface properties need to be enhanced by such processes to prevent degradation of bulk properties In this work, the surface of (Fe,Cr)-10%vol Al_2O_3 nanocomposite was treated by O_2 ion implantation. Oxygen is implanted into the material using a pulsed cathodic arc at ambient temperature and the surface modification, mechanical properties and oxidation behavior are systematically determined. This paragraph was added to the introduction concerning the effect of ion implantation on other nanocomposites.

2. Materials and methods

Samples of (Fe,Cr)Al-10%vol Al_2O_3 were prepared from raw materials by mechanical alloying for 100 h, followed by hot pressing for 15 min at 1600 °C, under a pressure of 5.5 GPa in a vacuum atmosphere [2]. The bulk specimens were 10 mm in diameter and 5 mm in thickness. The (Fe,Cr)Al-10%vol Al_2O_3 nanocomposites were polished using silicon carbide papers of 600, 1200, 2500 and 4000 grit and final polishing was performed using diamond and alumina paste in order to produce a scratch-free mirror-finished surface. Ion implantation was carried out in a GPI-100 ion beam implanter with an ECR source for oxygen; when plasma was excited with 2.45 GHz microwaves and input power of 200–900 W, an O_2 was formed with dose of 1×10^{18} ions/cm^2 in the chamber using an oxygen flow rate of 20 sccm. Pulsed voltage, pulse width and pulsing frequency were 150 kV, 20 μs, and 100 Hz, respectively, and implantation was conducted for a duration of 3 h. The aluminum sample holder on which the (Fe,Cr)-10%vol Al_2O_3 bulk samples were positioned 5 cm beneath the RF source. The sample holder was mounted onto the bottom of the vacuum chamber, electrically isolated from the chamber. The instrument was pumped down to a base pressure of 1×10^{-6} Torr before oxygen gas was fed into the chamber. During processing of the specimens, the working pressure was set at 0.1 Torr and RF power was 900W.

Atomic force microscopy (AFM) in contact mode was used to determine the surface topography and roughness. Phase constituents were identified by using X-ray diffractometry with a Cu K_α radiation. Transmission electron microscope (FEI Tecnai G220 Scanning TEM) and scanning electron microscope (LEO 1530 SEM) with an electron backscattered diffraction (EBSD) analyzer were applied for characterization of microstructure and texture. FEI Quanta 200 was used to produce TEM foils from the bulk sample. Nano-hardness and scratch tests were performed using an Agilent Nano Indenter G200 equipped with a Berkovich tip and XP transducer that combines load and displacement resolutions with unmatched flexibility in load 20 mN and displacement ranges. The oxidation investigation was performed in an electrical muffle furnace at 1100 °C for 100 h; weight changes of the nanocomposite specimens, un-implanted and oxygen implanted, were recorded every 10 h after cooling down to room temperature.

3. Results and discussion

3.1. Microstructure and phase analysis

During oxygen ion implantation, oxygen atoms are first ionized so that each has a positive and negative charge. Through the use of electric and magnetic fields, the ions are focused into a well-defined beam and accelerated to very high energies under vacuum. Then the beam is scanned in a raster on the surface of the nanocomposite. By this means, the distribution of ions over the nanocomposite surface is made very uniform. Due to high accelerating voltage, the ions have sufficient energy to penetrate into the (Fe,Cr)Al, giving up their energies by colliding with lattice atoms or their electrons until, finally, they come to rest. It must be noted that when an ion stops moving, it unites with an electron in the host and again becomes a dopant atom; it is said that the dopant atom has been implanted into the (Fe,Cr)Al. Since Al_2O_3 formation has the lowest Gibbs free energy compared to Fe_2O_3 and Cr_2O_3, oxygen ions react with Al^{+3} to form aluminum oxide; Al_2O_3 is the only oxide of aluminum that is stable with respect to oxygen loss during bombardment. Al atoms in Al_2O_3 structure with correct stoichiometry, and strong bond energy is less affected by O ions bombed onto the surface in comparison with Al in (Fe,Cr)Al intermetallic compound. XRD patterns of (Fe,Cr)Al-10%vol Al_2O_3 nanocomposite specimens, before and after O_2 ion implantation, are presented in Fig. 1. The patterns reveal that the structure is mainly composed of Al_2O_3 and (Fe,Cr)Al phases. The results did not exhibit any significant difference in the phase compositions, but, Al_2O_3 peaks had higher intensities in the ion implanted sample, most probably due to formation of more Al_2O_3 during oxygen implantation. Aluminum oxide has two main forms; alpha-Al_2O_3 with hexagonal structure and gama-Al_2O_3 with cubic structure. It has been stated that amorphous alumina would transform to γ-Al_2O_3 at temperatures above 375 C [30]. Initially, during oxygen ion bombardment of low doses, Al_2O_3 precipitates are formed within the surface layers and then, at higher doses, a thin layer of Al_2O_3 covers the specimen surface. Results of x-ray diffraction in Fig. 1 indicates that this phase is α-Al_2O_3; such aluminum oxide is stable with respect to oxygen loss during ion bombardment, although it has been argued that

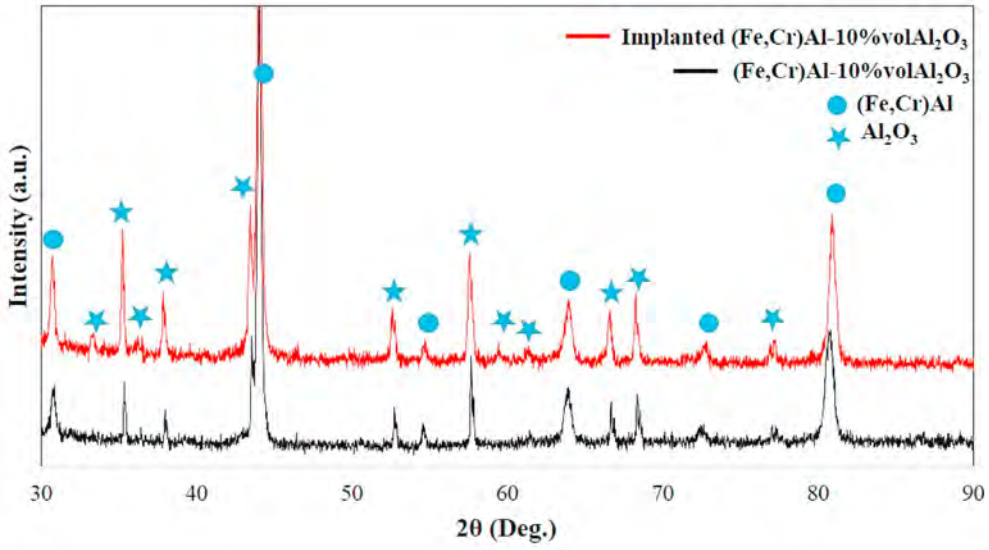

Fig. 1. XRD patterns of the (Fe,Cr)Al-10%vol Al_2O_3 samples, as-received and after O_2 ion implantation.

Al_2O_3 formed at room temperature by ion implantation could be partially amorphous [30].

The implanted oxide layer formation can be envisioned to occur in bulks containing aluminum as follows: (a) low ion doses result in Al_2O_3 precipitates increasing with ion dose; (b) at doses approaching that required for saturation (i.e., oxidation of all the locally available aluminum atoms), the precipitates coalesce forming a low density Al_2O_3 layer containing some metallic aluminum inclusions and some oxygen physically trapped at point defects and/or microvoids; (c) for doses greater than that required to oxidize essentially all the metallic aluminum inclusions, the concentration of trapped oxygen increases because the diffusion rate near room temperature is too low for the oxygen to diffuse readily to Al_2O_3/(Fe,Cr)Al interfaces; and (d) additional increases in the oxygen dose serve to increase the radiation damage at the surface side of the layer and enhance the mobility of the trapped oxygen; it can escape that region of the layer, leaving a chemically stable, densified, stoichiometric region. For all doses, oxygen is initially implanted in an oxide phase, slowly diffuses and upon reaching an interface reacts with the aluminum to form Al_2O_3, thereby, increasing the thickness of the implanted layer. Diffusion through the densified, amorphous region should be slower than that of the lower density region at greater depths. This could explain the apparently fast growth of the implanted layer at the deep Al-included interface [4–7,13]. Fig. 2 reveals AFM images of un-implanted and O_2 ion implanted (Fe,Cr)Al-10%vol Al_2O_3 nanocomposites. As it is seen, after implantation, surface topology and roughness are both changed; the surface roughness of un-implanted specimen was 292 nm, whereas after implantation it decreased to 236 nm. Hence, it can be stated that a relatively smoother surface is formed after the bombardment of specimen by oxygen ions.

SEM micrographs and EDS analysis of O_2 ion implanted (Fe,Cr)Al–Al_2O_3 nanocomposites are shown in Fig. 3 and Table 1. The black and gray phases appeared in Fig. 3 are related to alumina and (Fe,Cr)Al phases, respectively [2]. In our previous paper [2], EDS analysis indicated that (Fe,Cr)Al includes two main phases: 1) high Cr phase (dark gray), 2) low Cr phase (light gray). It is obvious that the black phase, Fig. 3b, has been increased compared with Fig. 3a; these evidences confirm that the amount of oxygen in the ion implanted layer is increased compared with that of the un-implanted surface.

Fig. 4 compares EBSD patterns of un-implanted and O_2 ion implanted specimens; the blue and red phases belong to Al_2O_3 and (Fe,Cr)Al, respectively. An increase in the fraction of Al_2O_3 phase, without formation of any new phases, is caused by O_2 implantation

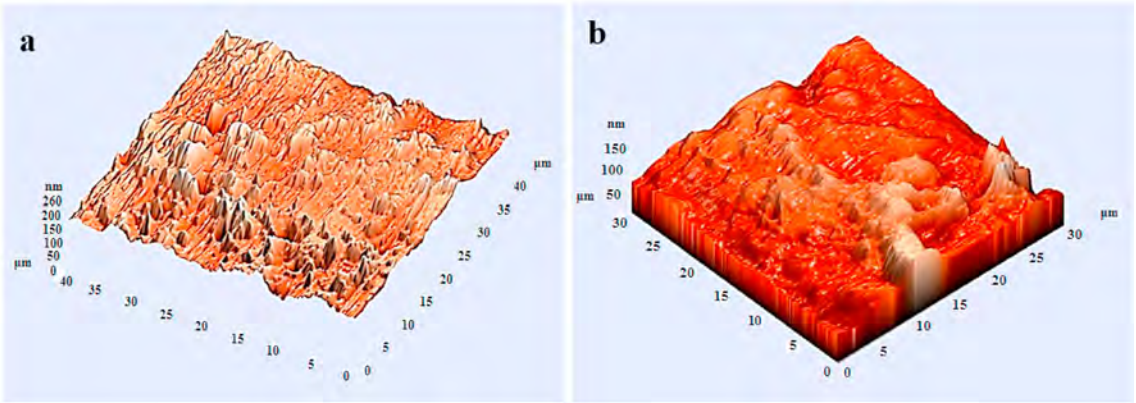

Fig. 2. AFM images of (a) un-implanted and (b) O_2 ion implanted (Fe,Cr)Al-10%vol Al_2O_3 nanocomposite.

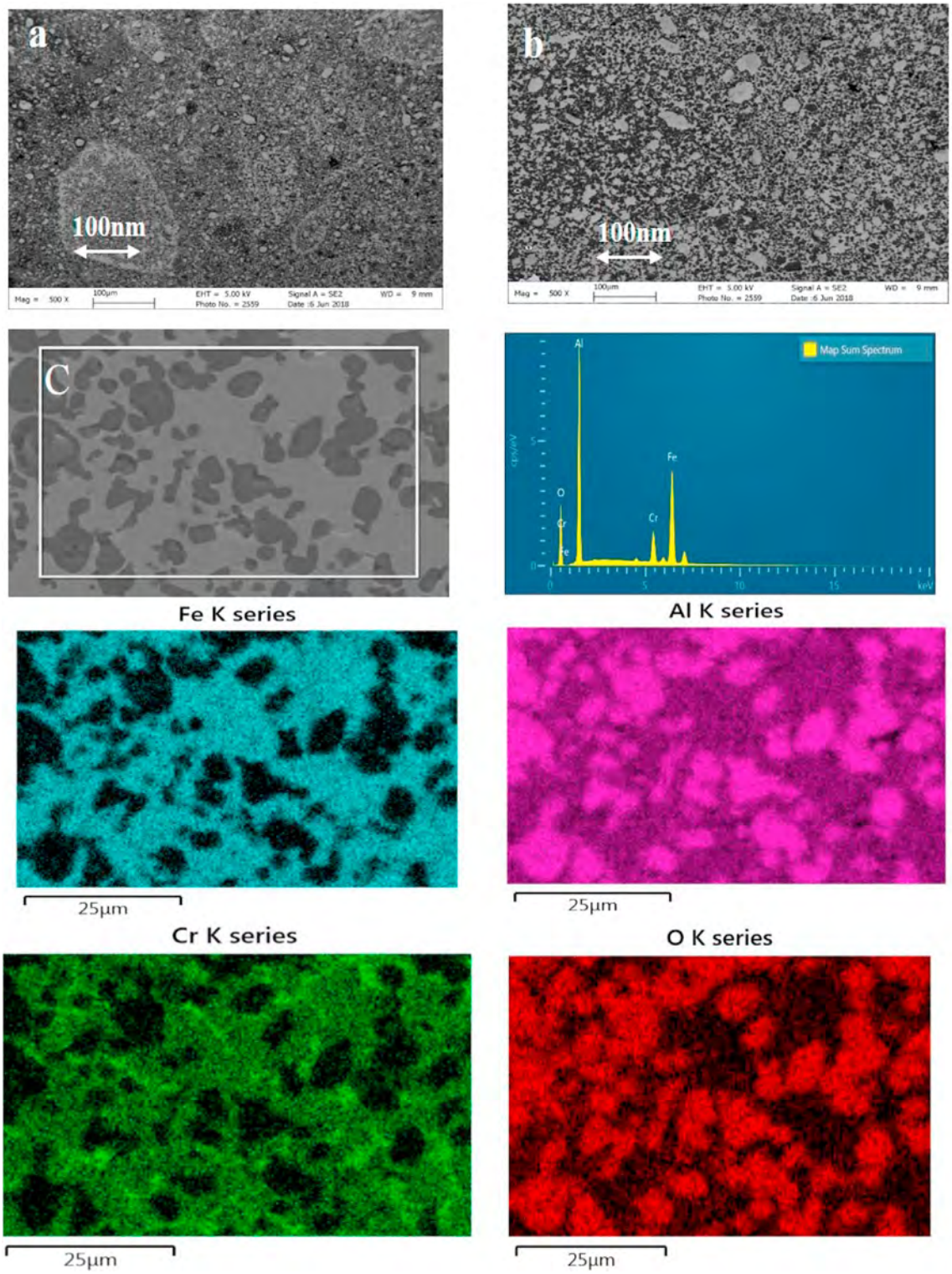

Fig. 3. SEM micrographs of (a) un-implanted (b) O_2 ion implanted specimens, (c) EDS elemental maps of (Fe,Cr)Al-10%vol Al_2O_3 nanocomposite after O_2 ion implantation.

process. The results are similar to those obtained by Loinaz et al. [20] using conventional ion implantation of nitrogen, carbon or oxygen.

Fig. 5 (a) represents a TEM images of O_2 ion implanted layer on the surface of (Fe,Cr)Al-10%vol Al_2O_3 nanocomposite. It signifies the formation of a thin layer with a new composition on the surface of the nanocomposite; the new composition is the fine-grained alumina layer with a uniform distribution on the surface. The size and distribution of Al_2O_3 nanoparticles in the microstructure are shown in Fig. 5b. To measure the size of the Al_2O_3 particles observed in this photo, we used the microscopic image processing software ImageJ, to draw the outline of each distinguishable particle and measure the area enclosed in the outline. Fig. 6a shows a transmission electron microscope (TEM) image of ion-implanted

Table 1
EDS microanalyses of the surface layer of (Fe,Cr)Al-10%volAl_2O_3 nanocomposite.

Element	Line Type	un-implanted		O_2 ion implanted	
		wt%	at %	wt%	at %
O	K series	4.42	10.75	8.62	20.02
Al	K series	29.74	42.86	26.12	35.97
Cr	K series	10.76	8.05	11.83	8.46
Fe	K series	55.08	38.34	53.43	35.56
Total:		100.00	100.00	100.00	100.00

(Fe,Cr)Al−Al_2O_3 nanocomposite after filtering the image to eliminate random noise and finding the threshold value for image segmentation (separation into foreground and background). Segmenting the image based on this threshold value that allows fully define the object by ImagJ. During the particle counting procedure, a threshold must be applied to distinguish the particles from the substrate. The size distribution of the Al_2O_3 particles (Fig. 6b) indicated that the majority of particles sizes are about 50−70 nm in agreement with Al_2O_3 particle size estimated using Williamson-Hall method [2] and TEM images Fig. 5b.

3.2. Mechanical properties

Nano-hardness tests were carried out in the load-controlled mode with a Berkovich tip at a maximum load of 20 mN. Fig. 7 illustrates loading-unloading curves; the nanoindentation tests performed on the O_2 ion implanted samples revealed an obvious increase in hardness compared to the un-implanted nanocomposite. The nanohardness, Young's modulus and fracture toughness for the un-implanted and O_2 ion implanted (Fe,Cr)Al-10% vol Al_2O_3 nanocomposites are summarized in Table 2. The high hardness (33.2 GPa) obtained on the implanted surface can be assigned to the increase in fraction of the fine-grained alumina phase and its uniform distribution within the outermost layer (Fig. 5). The results indicated that O_2 ion implantation improved the Young's modulus of the top surface layers of (Fe,Cr)Al-10%vol Al_2O_3 from 607 to 846 GPa; an increase of about 40% in elastic modulus would enhance the elastic behavior of surface and, in turn, load bearing capacity of the material. Thus, coefficient of friction and wear characteristics of the implanted nanocomposite are positively affected. To estimate the fracture toughness, K_{IC} was measured by nanoindendation test; according to Fig. 8, no crack was observed

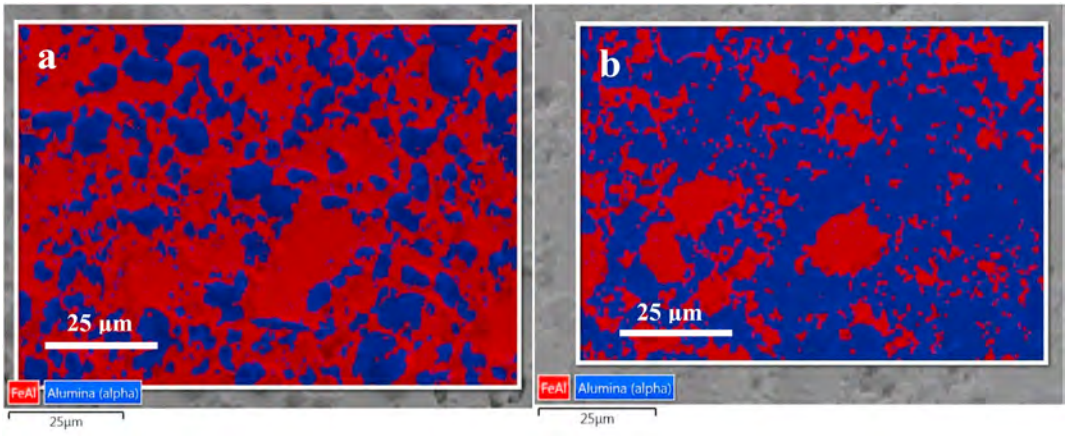

Fig. 4. Phase distribution by EBSD analysis on the surface of (a) un-implanted and (b) O_2 ion implanted (Fe,Cr)Al-10%vol Al_2O_3 nanocomposite.

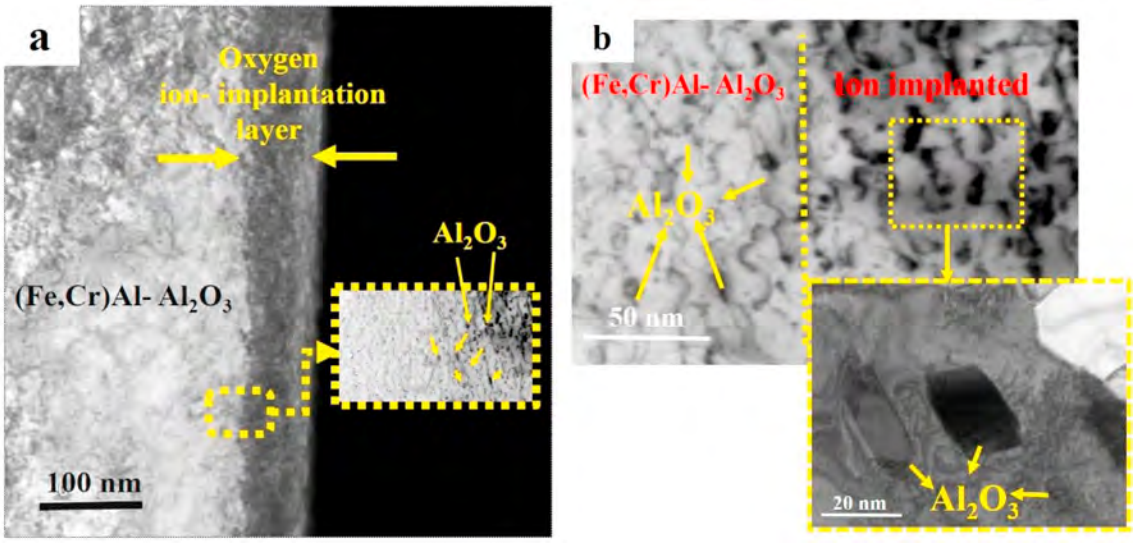

Fig. 5. Bright-field TEM micrographs of samples, (a) O_2 ion implanted layer on the surface of (Fe,Cr)Al-10%vol Al_2O_3 nanocomposite and (b) Distribution and size of Al_2O_3 nanoparticles.

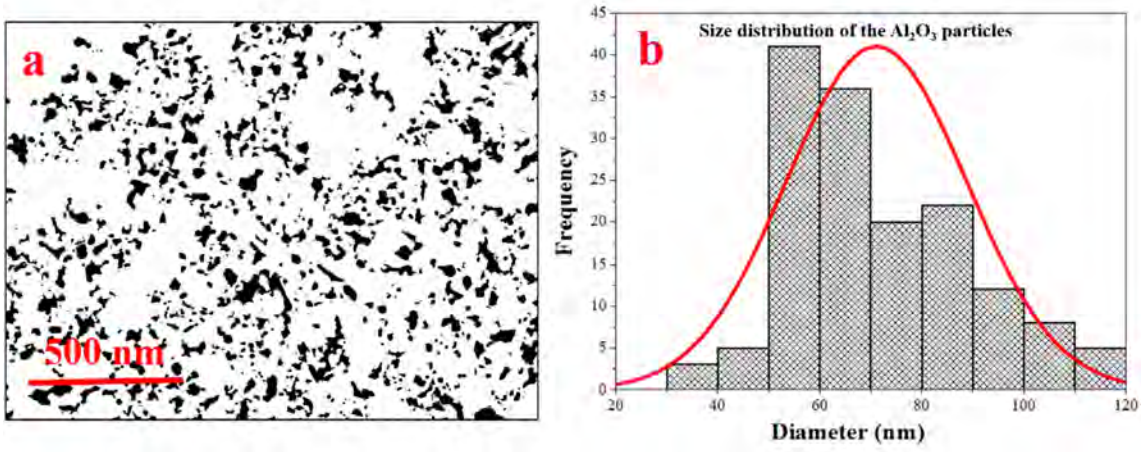

Fig. 6. (a) TEM image of ion-implanted (Fe,Cr)Al–Al_2O_3, (b) Size distribution histogram graph and Gaussian fitting of Al_2O_3 nanoparticles using ImagJ software.

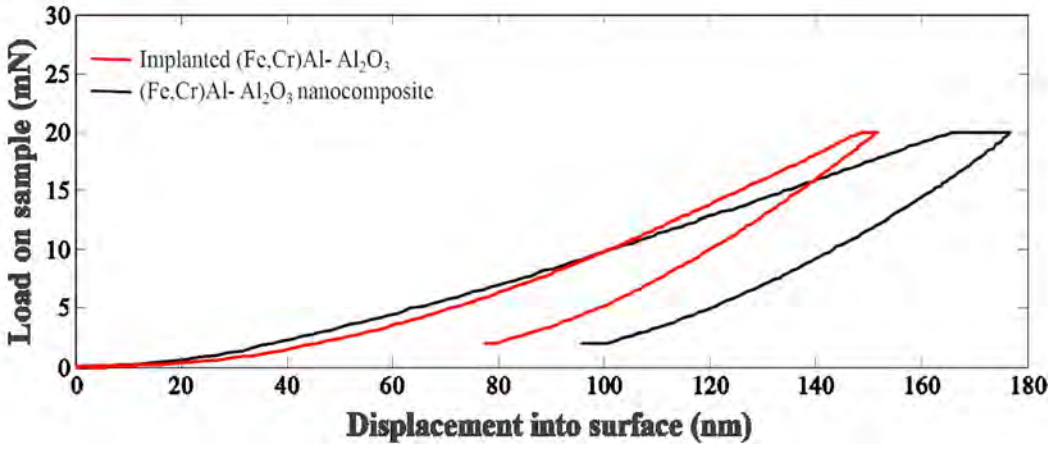

Fig. 7. Load – displacement curves of un-implanted and O_2 ion implanted (Fe,Cr)Al-10%vol Al_2O_3 nanocomposite obtained during nanoindentation testing to maximum load of 20 mN.

Table 2
Nano-hardness (H), Young's modulus (E) and fracture toughness of un-implanted and O_2 ion implanted nanocomposite samples obtained by nanoindentation tests.

Un-implanted			O_2 ion implanted		
Young's modulus (GPa)	Hardness at max load (GPa)	Fracture toughness (MPa.m$^{1/2}$)	Young's modulus (GPa)	Hardness at max load (GPa)	Fracture toughness (MPa.m$^{1/2}$)
607.2	21.7 ± 1.8	19.6 ± 0.4	696.0	33.2 ± 1.6	21.3 ± 0.9

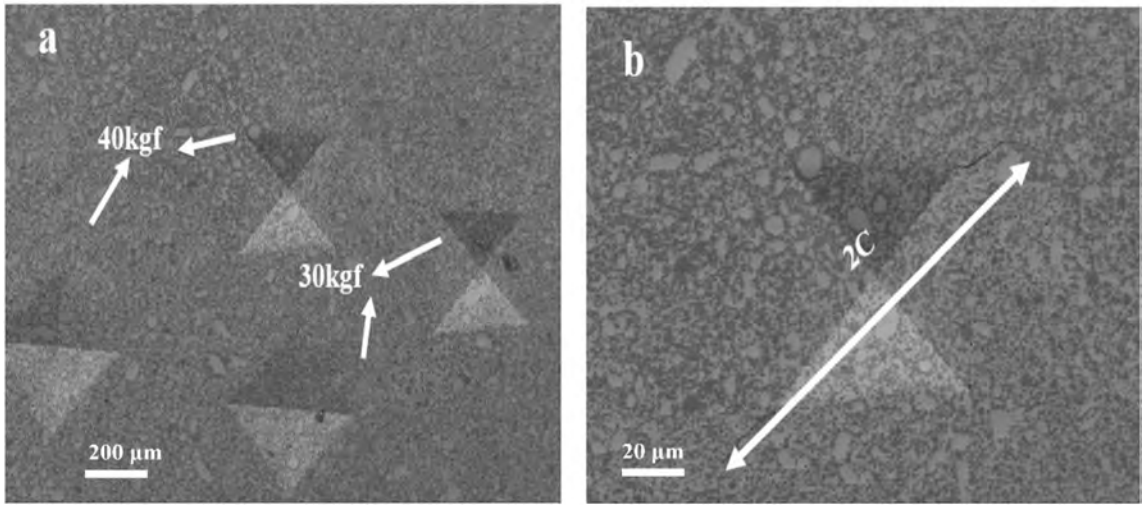

Fig. 8. SEM image of Vickers hardness indentation on O_2 ion implanted layer (a) at loads of 30 and 40 kgf, (b) crack propagation pattern under load of 50 kgf.

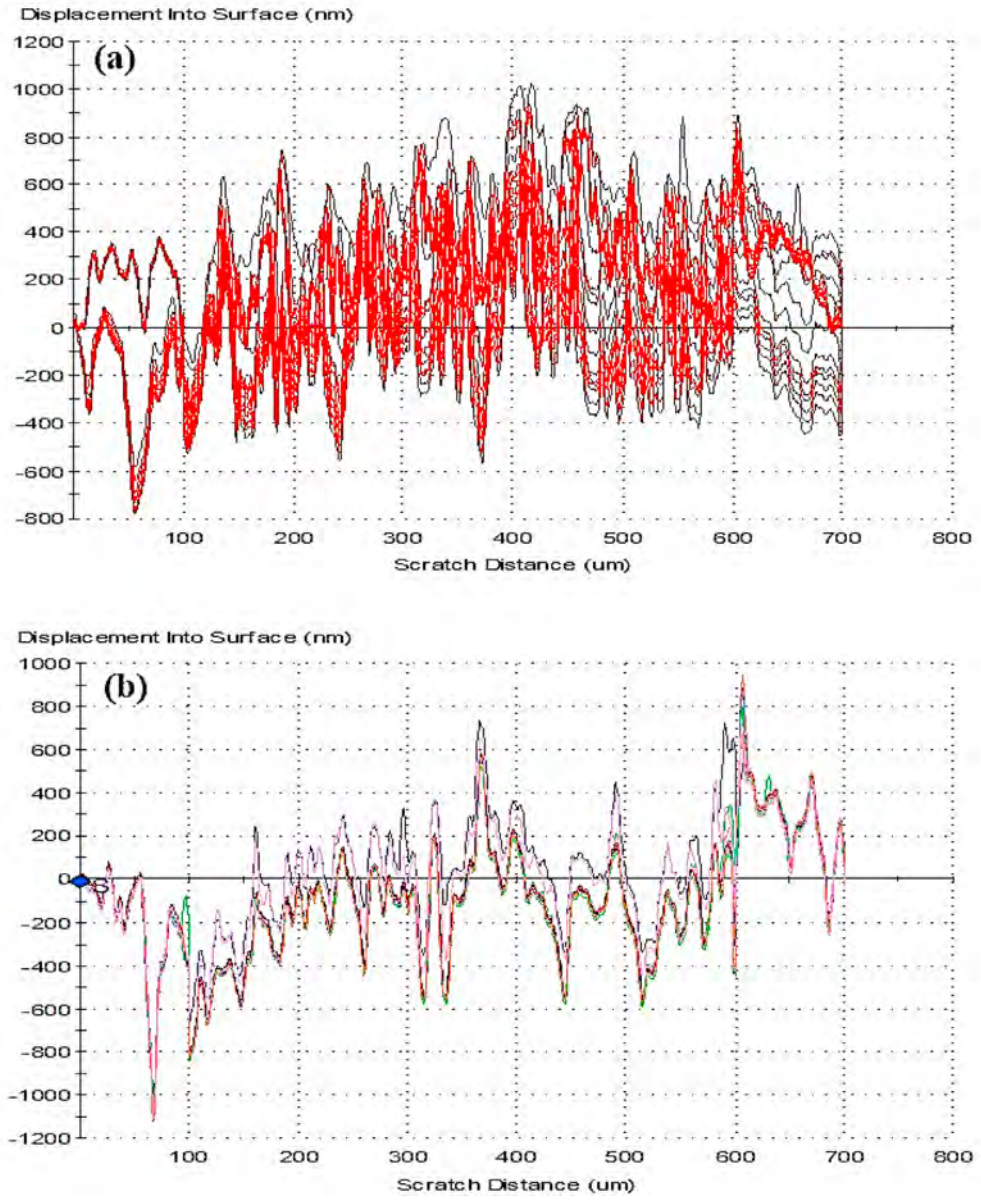

Fig. 9. Displacement into surface versus travel distance in scratch test; (a) untreated and (b) O_2 ion implanted nanocomposite.

Table 3
Results of scratch tests in single direction mode.

	Number of cycles	Wear track deformation **micron**^{2}	Average residual deformation during the return (nm)	Average coefficient of friction	Position for cross profile	Groove width (nm)	Residual groove depth (nm)	Total groove height (nm)
(Fe,Cr)Al−10% Al_2O_3	10	170	412	**0.11**	350	54	246	422
After ion implantation	10	162	379	**0.08**	350	43	195	368

with loads lower than 50 kgf. An increase of about 10% in fracture toughness (from 19.6 to 21.3 MPa $m^{1/2}$) for O_2 ion implanted nanocomposite was observed that can be due to an increase in fraction of hard Al_2O_3 phase in the implanted surface layers. The mechanisms involving toughness improvement by Al_2O_3 nanoparticles have been described in our previous work [2].

To study the effect of ion implantation on tribological behavior of (Fe,Cr)Al-10%volAl_2O_3 nanocomposite, scratch tests were conducted at load of 5 mN. Fig. 9 shows aligned displacement curves obtained by scratch testing where each specimen was scratched 5 times to ensure reproducibility of the results and a meaningful scatter in the data. Displacement into the surface of the implanted nanocomposite was lower than that of untreated substrate; the measurements revealed that both depth and width of the scratches

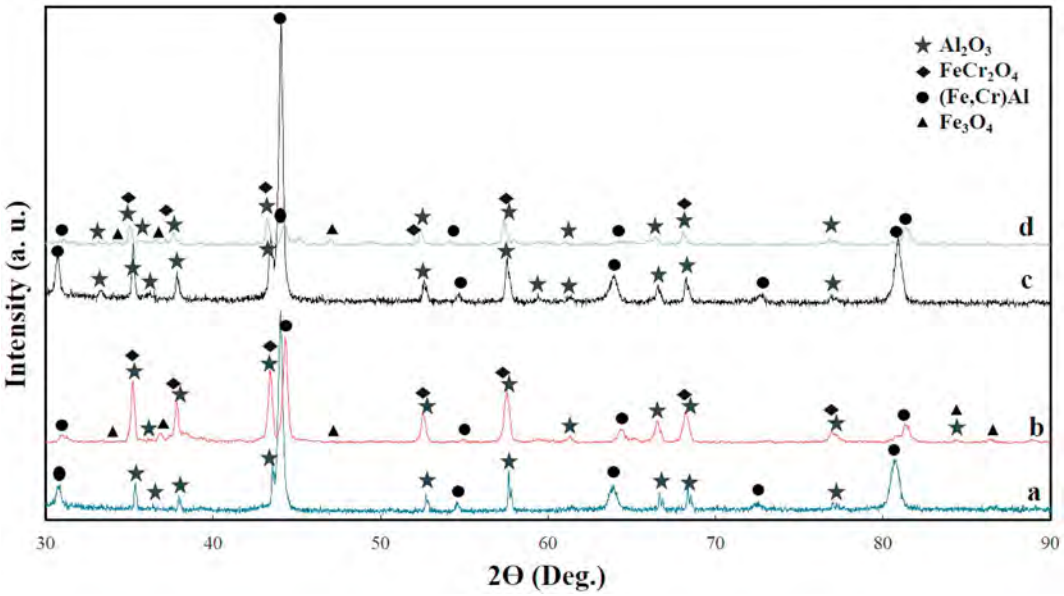

Fig. 10. XRD patterns of (Fe,Cr)Al-10%vol Al_2O_3 nanocomposite; (a) as-produced, (b) after 100 h oxidation at 1100 °C, (c) oxygen ion implanted, (d) after oxygen ion implanted and 100 h oxidation at 1100 °C.

had smaller sizes after oxygen implantation. Based on scratch tests data in Table 3, it can be stated that coefficient of friction of the nanocomposite was 0.11 which is reduced to 0.08 after ion implantation, tested under identical conditions. In addition, the size of the scratch groove indicates a significant decrease; these findings confirm the improvement in the mechanical properties as well as tribological characteristics of the nanocomposite as a result of oxygen ion implantation. The improvement is attributed to the increase in hardness and elastic modulus of the surface layers as well as higher percentage of oxide within the implanted volume. Nevertheless, due to thin nature of the ion implanted layer, the load bearing of the treated nanocomposite is limited to a depth of about 100 nm and, thus, the improvement in mechanical properties would be effective under the conditions that the applied stress is not too high to transmit deformation to underneath layers.

3.3. Oxidation resistance

Fig. 10 reveals the XRD patterns of un-implanted and oxygen implanted (Fe,Cr)Al-10%vol Al_2O_3 nanocomposite before and after cyclic oxidation testing at 1100 °C for 100 h. It may be observed that the peaks related to the substrate material and surface layer, namely (Fe,Cr)Al and Al_2O_3, are reduced in intensity after high temperature oxidation; an effect that is attributed to the formation of oxides on the nanocomposite surface. On the other hand, the intensity of peaks related to iron oxides (Fe_3O_4 and $FeCr_2O_4$), after 100 h oxidation, are lower for the ion implanted specimen compared to the un-implanted surface, indicating the protection of nanocomposite against high temperature oxidation by the implantation of oxygen ions. Further comparison of the peak intensities confirmed the formation of rather high amount of alumina phase in the ion implanted specimen; α-Al_2O_3 is a well-known phase in corrosion and oxidation protection due to its dense structure and chemical stability. It has been reported that alumina forming heat-resisting alloys exhibit excellent oxidation resistance in oxidizing atmospheres at temperatures up to 1573K as a result of a continuous layer of protective α-Al_2O_3 [31–33].

Surface morphology of un-implanted and O_2 ion implanted of the nanocomposite after oxidation at 1100 °C for 100 h are shown in Fig. 11. SEM examination of the surface topography revealed formation of rather coarse plate-like oxide scale on the nanocomposite (Fig. 11 a, b) and compacted particles of fine oxide on the implanted specimen (Fig. 11 c, d).

Quick growth of oxide particles on the surface of un-implanted nanocomposite caused not only high oxidation rate, but also formation of cracks on the un-implanted specimen after oxidation, displayed by white arrows in Fig. 11a. Sayyedan et al. [31] studied the high temperature oxidation behavior of an aluminum containing coating on stainless steel and found out that the outer most iron-rich oxide particles grow up rapidly with increasing the oxidation time, until finally detach from the surface due to excessive stress concentration and poor bonding between thickened oxide scale. Coarsening of the oxide particles followed by stress development and crack growth are the observed phenomena during high temperature oxidation of the (Fe,Cr)Al-10%vol Al_2O_3 nanocomposite. Oxygen ion implantation of the nanocomposite protected the surface at high temperature through formation of a rather dense layer of fine oxide particles; slower growth of the oxide scale means lower rate of oxidation of the material.

Analysis of data obtained in high temperature cyclic oxidation tests are presented in Fig. 12 which shows weight gain per unit area and the trend lines of kinetic curves versus oxidation time for ion implanted and un-implanted (Fe,Cr)Al-10%vol Al_2O_3 nanocomposite. According to experimental findings, the oxidation rates' curves for both un-implanted and ion implanted specimens include two stages, the first stage from 0 to 50 h follows the parabolic oxidation law given by Equation (1) and the second stage from 50 to 100 h follows the linear oxidation law given by Equation (2). These oxidation models are common for description of high temperature oxidation of a wide range of engineering alloys [31].

$$(\Delta W/A)^2 = a + k_p\, t \tag{1}$$

$$(\Delta W/A) = b + k_l\, t \tag{2}$$

In Equations (1) and (2), ΔW is the weight gain, A is the surface area, k_p is the parabolic rate constant, k_l is the linear rate constant, t is the oxidation time and a and b are a constant. Fig. 12a reveals that

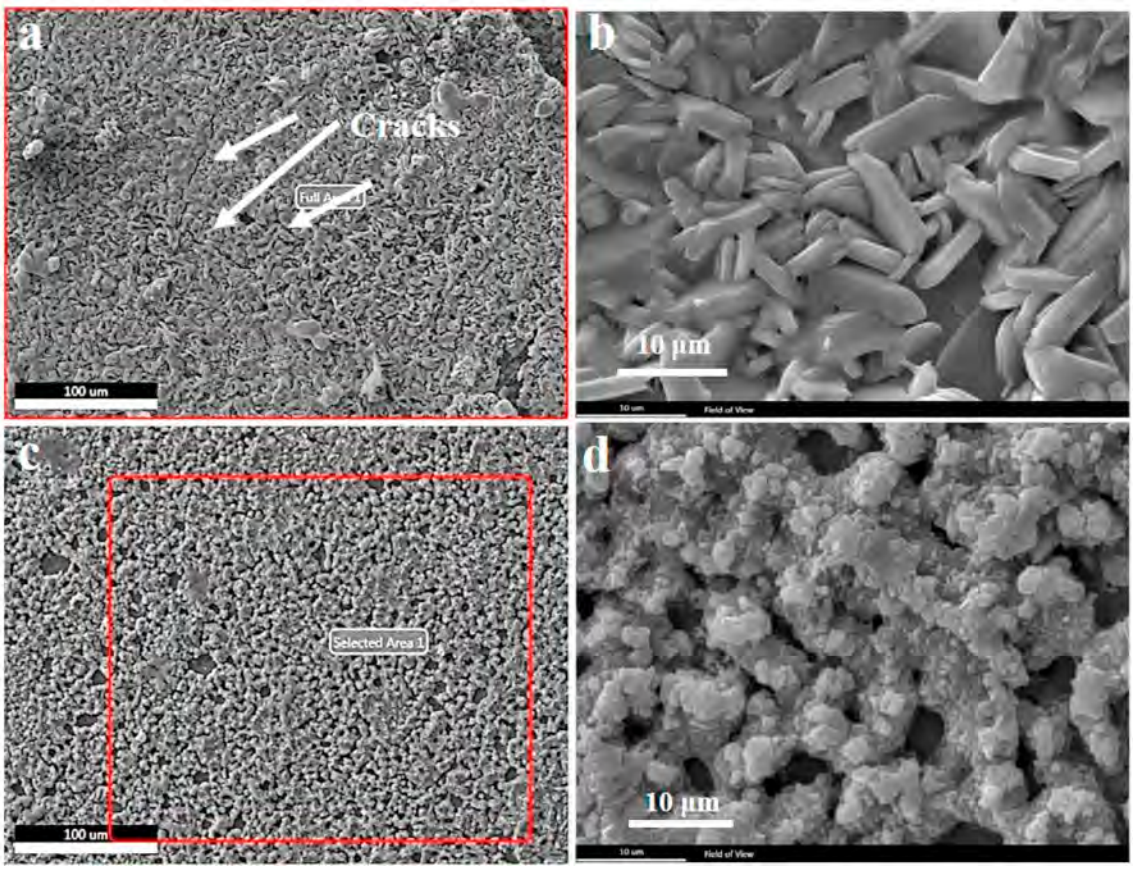

Fig. 11. SEM images of (a) and (b) (Fe,Cr)Al-10%vol Al_2O_3 nanocomposite after 100 h oxidation at 1100 °C, (c) and (d) O_2 ion implanted (Fe,Cr)Al-10%vol Al_2O_3 after 100 h oxidation at 1100 °C.

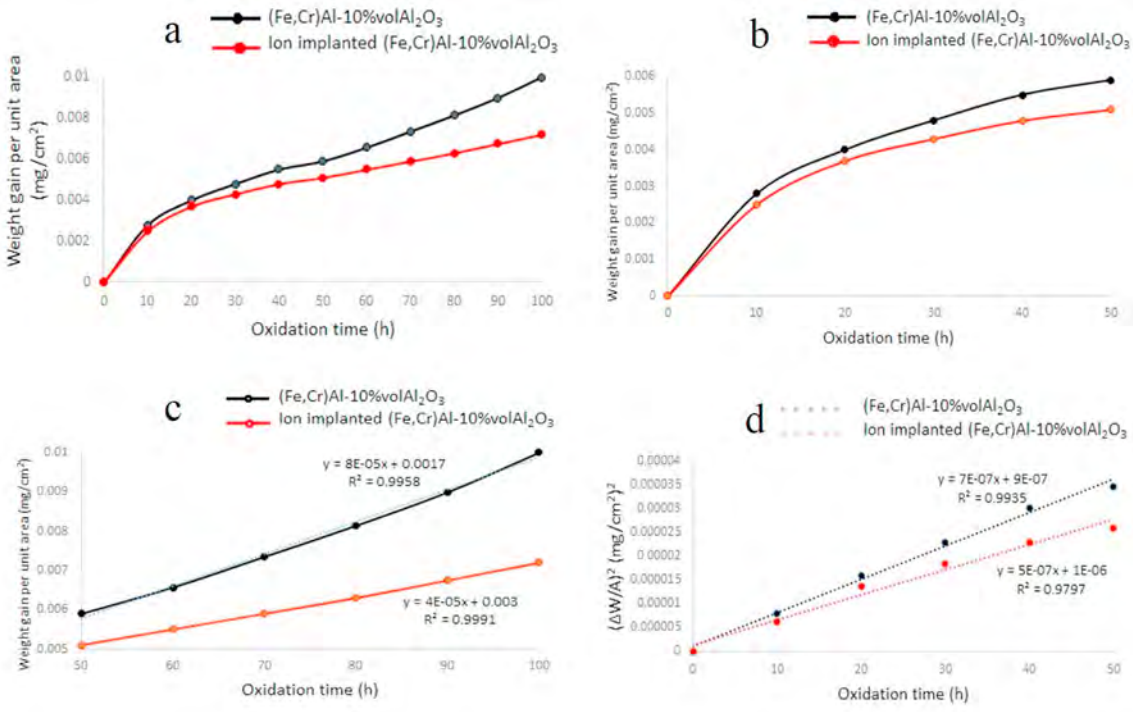

Fig. 12. (a) Weight gain per unit area (0–100 h), (b) Weight gain per unit area (0–50 h), (c) Weight gain per unit area (50–100 h), and (d) The trend lines of kinetic curves versus time for implanted and un-implanted (Fe,Cr)Al-10%volAl_2O_3 nanocomposite for 0–50 h cyclic oxidation at 1100 °C.

the weight gains per unit area of the ion implanted sample is lower than that of the un-implanted nanocomposite at all exposure times. The improvement in oxidation resistance is not very significant, but it is considerable. Moreover, kinetic curves related to 0–50 h oxidation period presented in Fig. 12d confirms that the parabolic rate constant for ion implanted specimen is 5×10^{-7}, while it is 7×10^{-7} for un-implanted sample, indicating a reduction of 28%. Also, Fig. 12c related to 50–100 h oxidation period indicates that the linear rate constant for ion implanted specimen is 4×10^{-5}, while it is 8×10^{-5} for un-implanted sample, indicating a reduction of 50%. It seems that the ion implanted layer is more capable of surface protection of the substrate in prolonged exposure times. Overall, evaluation of the high temperature oxidation of the un-implanted and ion implanted nanocomposites revealed slight improvement of oxidation resistance by the ion implantation process. Formation of a compact, uniform and fine-grained Al_2O_3 layer on the surface of (Fe,Cr)Al-10%vol Al_2O_3 is responsible for high temperature oxidation resistance of the modified nanocomposite [31].

4. Conclusions

- In the present study surface characteristics of (Fe,Cr)Al-10%vol Al_2O_3 nanocomposite were investigated and the influence of surface modification by O_2 ion implantation are reported.
- The nano-hardness and Young's modulus of the surface layers increase significantly as a result of oxygen implantation at 1×10^{18} ions/cm^2.
- The process improves tribological properties of the nanocomposite and, in particular, a reduction in coefficient of friction was achieved.
- Ion implantation caused a considerable increase in high temperature oxidation resistance of the nanocomposite, however, the improvement is not very significant.

CRediT authorship contribution statement

F. Sourani: Conceptualization, Methodology, Formal analysis, Investigation, Data curation, Writing - original draft, Visualization. **M.H. Enayati:** Conceptualization, Investigation, Writing - review & editing, Supervision. **F. Ashrafizadeh:** Conceptualization, Resources, Writing - review & editing, Visualization, Supervision. **F.S. Sayyedan:** Methodology, Validation, Investigation, Resources. **P.K. Chu:** Conceptualization, Investigation.

Declaration of competing interest

The authors declare that they have no known competing financial interests or personal relationships that could have appeared to influence the work reported in this paper.

Element	Line Type	un-implanted		O_2 ion implanted	
		wt%	at %	wt%	at %
O	K series	4.42	10.75	8.62	20.02
Al	K series	29.74	42.86	26.12	35.97
Cr	K series	10.76	8.05	11.83	8.46
Fe	K series	55.08	38.34	53.43	35.56
Total:		100.00	100.00	100.00	100.00

Un-implanted			O_2 ion implanted		
Young's modulus (GPa)	Hardness at max load (GPa)	Fracture toughness (MPa.m$^{1/2}$)	Young's modulus (GPa)	Hardness at max load (GPa)	Fracture toughness (MPa.m$^{1/2}$)
607.2	21.7 ± 1.8	19.6 ± 0.4	696.0	33.2 ± 1.6	21.3 ± 0.9

Acknowledgments

The authors would like to thank Isfahan University of Technology for provision of this work and Mechanical Engineering Laboratory of the University of Hong Kong in providing research facilities.

References

[1] M.H. Enayati, M. Salehi, Formation mechanism of Fe_3Al and FeAl intermetallic compounds during mechanical alloying, Mater. Sci. 40 (2010) 3933–3938.
[2] F. Sourani, M.H. Enayati, X. Zhou, S. Wang, A.H.W. Ngan, Nanoindentation behavior of nanostructured bulk (Fe,Cr)Al and (Fe,Cr)Al-Al_2O_3 nanocomposites, J. Alloys Compd. 792 (2019) 348–356.
[3] S.E. Aghili, M.H. Enayati, F. Karimzadeh, Synthesis of nanocrystalline (Fe,Cr)3Al powder by mechanical alloying, Mater. Manuf. Process. 27 (2012) 467–471.
[4] J. Zhu, H. Peng, F. Wang, Synthesis, microstructure and mechanical properties of (Ti,Mo)Al/Al_2O_3 in situ composites by reactive hot pressing, Mater. Res. Stand. 32 (2017) 1129–1137.
[5] F. Wang, Y. Zhaon, C. Yang, N. Fan, J. Zhu, Effect of MoO_3 on microstructure and mechanical properties of (Ti,Mo)Al/Al_2O_3 composites by in situ reactive hot pressing, Ceram. Int. 42 (2016) 1–8.
[6] J.F. Zhu, L. Ye, L.H. He, Effect of Al_2O_3 on the microstructure and mechanical properties of Ti_3AlC_2/Al_2O_3 in situ composites synthesized by reactive hot pressing, Ceram. Int. 38 (2012) 5475–5479.
[7] P. Kittali, J. Satheesh, G.A. Kumar, T. Madhusudhan, A review on role of reinforcements on mechanical and tribological behavior of aluminum based metal matrix composites, J. Eng. Technol. 3 (2016) 2412–2416.
[8] S.E. Aghili, M.H. Enayati, F. Karimzadeh, Fabrication of bulk $(Fe,Cr)_3Al/Al_2O_3$ intermetallic matrix nanocomposite through mechanical alloying and sintering, Acta Metall. 29 (2016) 911–919.
[9] R. Subramanian 1, C.G. McKamey, J.H. Schneibel, L.R. Buck, P.A. Menchhofer, Iron aluminide–Al_2O_3 composites by in situ displacement reactions: processing and mechanical properties, Mater. Sci. Eng A254 (1998) 119–128.
[10] Y.P. Bai, J.D. Xing, S.Q. Ma, Q. Huang, Y.Y. He, Z. Liu, Y.M. Gao, Static corrosion behavior of in-situ nanocrystalline Al_2O_3/Fe(Al) composites, Surf. Rev. Lett. 24 (2017) 1750029–1750040.
[11] W. Jin, P.K. Chu, Surface functionalization of biomaterials by plasma and ion beam, Surf. Coating. Technol. 336 (2018) 2–8.
[12] M.I. Guseva, M.V. Atamanov, G.V. Gordeeva, V.E. neumoin, B.n. Choi, W. Kim, j.G. Han, Hardening of WC-Co alloys by ion implantation, Radiat. Eff. Defect. S, 138, 1996, pp. 57–62.
[13] V. Muthukumaran, M. Senthil kumar, V. Selladurai, Improvement of surface properties of AISI 316L SS by O2 and helium ion implantation, J. Eng. Des. Technol. 11 (2013) 34–43.
[14] M.C. Salvadoria, F.S. Teixeira, L.G. Sgubin, M. Cattani, I.G. Brown, Surface modification by metal ion implantation forming metallic nanoparticles in an insulating matrix, Appl. Surf. Sci. 310 (2014) 158–163.
[15] S. Barison, G. Battaglin, R. Bertoncello, E. Cattaruzza, A. Mascolo, P. Mazzoldi, M. Ruzzid, F. Trivillina, Composite materials obtained by ion irradiation: Mn implantation in silica glass, J. Mater. Chem. 9 (1999) 2929–2933.
[16] A. Meldrum, F. Richard, Jr. Haglund, A. Lynn, Boatner, C.W. White, Nanocomposite materials formed by ion implantation, Adv. Mater 13 (2001) 1431–1444.
[17] A.L. Stepanov, S.N. Abdullin, V.Yu Petukhov, YuN. Osin, R.I. Khaibullin, I.B. Khaibullin, Formation of metal-polymer composites by ion implantation, Philos. Mag. A B 80 (2000) 23–28.
[18] Y.C. Zhu, S. Ohtani, Y. Sato, N. Iwamoto, Influence of boron ion implantation on the oxidation behavior of CVD-SiC coated carbon-carbon composites, Carbon 38 (2000) 501–507.
[19] A. Shanaghi, P.K. Chu, Enhancement of mechanical properties and corrosion resistance of NiTi alloy by carbon plasma immersion ion implantation, Surf. Coating. Technol. 365 (2019) 52–57.
[20] A. Loinaz, M. Rinner, F. Alonso, J.I. Onate, W. Ensinger, Effects of plasma immersion ion implantation of O_2 on mechanical properties and microstructure of Ti6Al4V, Surf. Coating. Technol. 103–104 (1998) 262–267.

[21] H. Wu, G. Wu, P.K. Chu, Effects of cerium ion implantation on the corrosion behavior of magnesium in different biological media, Surf. Coating. Technol. 306 (2016) 6–10.
[22] T. Chen, E. Castanon, G. Jonathan, Gigax, H. Kim, R. Balerio, J. Fan, F.A. Garner, L. Shao, Nitrogen ion implantation into pure iron for formation of surface nitride layer, Nucl. Instrum. Methods Phys. Res. B 451 (2019) 10–13.
[23] H.H. Huang, D.K. Shiau, C.S. Cheni, J.H. Chang, S. Wang, H. Pan, M.F. Wu, Nitrogen plasma immersion ion implantation treatment to enhance corrosion resistance, bone cell growth, and antibacterial adhesion of Ti-6Al-4V alloy in dental applications, Surf. Coating. Technol. 365 (2019) 179–188.
[24] S. Mändl, D. Manova, Modification of metals by plasma immersion ion implantation, Surf. Coating. Technol. 365 (2019) 83–93.
[25] P. Vlcak, J. Fojt, Z. Weiss, J. Kopeček, V. Perina, The effect of nitrogen saturation on the corrosion behavior of Ti-35Nb-7Zr-5Ta beta titanium alloy nitrided by ion implantation, Surf. Coating. Technol. 358 (2019) 144–152.
[26] A.I. Ryabchikov, E.B. Kashkarov, A.E. Shevelev, A. Obrosov, D.O. Sivin, Surface modification of Al by high-intensity low-energy Ti-ion implantation: microstructure, mechanical and tribological properties, Surf. Coating. Technol. 372 (2019) 1–8.
[27] A.R. Marcondes, M. Ueda, K.G. Kostov, A.F. Beloto, N.F. Leite, G.F. Gomes, C.M. Lepienski, Improvements of ultra-high molecular weight polyethylene mechanical properties by nitrogen plasma immersion ion implantation, Braz. J. Phys. 34 (2004) 1667–1672.
[28] R. Tyagi, P. Davim, Processing Techniques and Tribological Behavior of Composite Materials, first ed., IGI Global, Pennsylvania, 2015.
[29] F. Sourani, M.H. Enayati, A.H.W. Ngan, On the insitu synthesis of (Fe,Cr)Al and (Fe,Cr)Al-Al_2O_3 nanostructured materials, Mater. Res. Express 6 (2019), 0850c9.
[30] R.G. Musket, D.W. Brown, H.C. Hayden, Formation of subsurface Al_2O_3 layer in aluminum by oxygen ion implantation, Nucl. Instrum. Methods. Phys. B7/8 (1985) 31–37.
[31] T. Amano, High- temperature oxidation resistance of Al_2O_3 and Cr_2O_3 forming heat-resisting alloys with noble metal and rare earths, Ecs Transactions 25 (2010) 3–19.
[32] F.S. Sayyedan, M.H. Enayati, Evaluating oxidation behavior of amorphous aluminum phosphate coating, Appl. Surf. Sci. 455 (2018) 821–830.
[33] G. Dearnaley, J.D. Benjamin, W.S. Miller, L. Weidman, The use of ion implantation in a comparison of the thermal oxidation, Titanium Zirconium 16 (1976) 717–728.